Morphology, Structure, and Kinetic Analysis of Nonisothermal Cold- and Melt-Crystallization of Syndiotactic Polystyrene

Jiali Cai,[1,2] Ying Han[1]

[1]*Key Laboratory for Ultrafine Materials of Ministry of Education, School of Materials Science and Engineering, East China University of Science and Technology, Shanghai 200237, People's Republic of China*
[2]*Key Laboratory of Mesoscopic Materials Science, College of Chemistry and Chemical Engineering, Nanjing University, Nanjing 210093, People's Republic of China*

Received 24 December 2005; accepted 19 June 2006
DOI 10.1002/app.25306
Published online in Wiley InterScience (www.interscience.wiley.com).

ABSTRACT: Nonisothermal cold- and melt-crystallization of syndiotactic polystyrene (sPS) were carefully carried out by Perkin–Elmer Diamond differential scanning calorimetry, polarized optical microcopy (POM), and wide angle X-ray diffraction. The experimental data subjected to the two types of processing were thoroughly analyzed on the basis of Avrami, Tobin, Ziabicki, and combination of Avrami and Ozawa models. Avrami, Tobin, and Ziabicki analyses indicate that nonisothermal cold-crystallization (A) characterizes smaller Avami and Tobin exponent and larger Ziabicki kinetic crystallizability index G than those obtained from nonisothermal melt-crystallization (B) possibly due to the existence of partially ordered structures in the quenched samples. Kissinger and the differential isoconversional method (DICM) of Friedman's were utilized to obtain effective energy barrier of A, in good agreement with that obtained by using Arrhenius equation to analyze the isothermal cold-crystallization, indicating that Kissinger and Friedman equations can be applied to obtain activation energy from A of sPS. X-ray diffraction analysis indicates that cold-crystallization mainly produces α-type crystal but for melt-crystallization the contents of α-type and β-type crystals depend on the cooling rates. The POM also indicates the difference of end morphology of the sample between A and B. At the same time, the DICM of Friedman's was applied to analyze experimental data of B, which were divided into two groups with 20 K/min as the threshold, and it was found that the formation of β-type crystal possesses larger absolute value of effective activation barrier than the formation of α-type crystal. © 2006 Wiley Periodicals, Inc. J Appl Polym Sci 103: 1311–1324, 2007

Key words: syndiotactic polystyrene; nonisothermal crystallization; activation energy; differential scanning calorimetry; polarized optical microscopy; X-ray diffraction

INTRODUCTION

Since when the successful synthesis of syndiotactic polystyrene (sPS) was reported in 1986,[1] it has been widely studied and has found applications in many fields. Till now, much attention has been paid to complex polymorphism and multiple melting endotherms.[2–5] In a general way, there exist four crystal forms (i.e., α, β, γ, δ) obtained by varying thermal processing conditions or solvent treatments. α and β forms with zigzag planar chain conformation could be obtained by melt- and cold-crystallization, while γ and δ forms with helical conformation could be formed in the presence of solvents such as benzene, toluene, etc.

Cimmino et al.[6] indicated that nucleation rate of sPS is rapid, exceeding that of iPS. Wesson[7] studied the nonisothermal crystallization kinetics of sPS samples with different molecular weights, using differential scanning calorimetry (DSC), indicating that the crystallization rate of sPS depends on the molecular weight.

Cold-crystallization is when amorphous polymer crystallizes at temperatures above T_g. During cold-crystallization, the polymer chains in the rubber state complete the corresponding conformation rearrangement via cooperative segmental movements, while for melt-crystallization, the motion of polymer chains can be performed by molecular reptation.[8,9] For this reason, the crystal structure obtained from cold-crystallization may be different from melt-crystallization. Woo et al.[10] studied the crystal structures and found that cold-crystallized sPS only yields one melting peak, attributed to α modification; while melt-crystallized sPS yields three melting peaks, attributed to α (peaks II and III) and β (peak I) modifications.

Although lots of crystallization studies related to sPS have been performed,[2–14] there is less work to directly analyze and compare the kinetic processes of nonisothermal cold- and melt-crystallization of one same sPS sample. In this contribution, we detailedly

Correspondence to: J. Cai (jlcai@ecust.edu.cn).
Contract grant sponsor: National Natural Science Foundation of China; contract grant number: 20574018.

investigated and contrasted nonisothermal cold- and melt-crystallization processes, and corresponding morphology and structures of the same sPS sample in full. The experimental data, for cold-crystallization with different cooling rates ranging from 2.5 to 60°C/min, and for melt-crystallization with different cooling rates ranging from 5 to 80°C/min were obtained from DSC technique and were thoroughly analyzed based on Ziabicki, modified Avrami, Tobin, and the combination of Avrami and Ozawa models. The effective energy barrier describing the nonisothermal crystallization processes of sPS was estimated based on Kissinger equation and the differential isoconversional method of Friedman, respectively. At the same time, polarized optical microcopy (POM) and X-ray diffraction techniques were utilized to investigate the morphology and structures.

EXPERIMENTAL

Material

The syndiotactic polystyrene (sPS) samples were provided by Dow Chemical. The molecular weight (M_w) of the sPS sample is 2.5×10^5 and $M_w/M_n = 2.6$, measured by high temperature GPC after dissolving the sample in trichlorobenzene (TCB) at 150°C. The syndiotacticity was about 97% ([rrr]). Glass transition and melting point of the sample was measured to be 100 and 270°C, respectively.

Sample preparation and experimental details

Differential scanning calorimetry

The sheets of the sPS samples were prepared by pressing the as-received granules at 320°C between polytetrafluoroethylene films and quickly placing the pressed sheets into liquid nitrogen. The obtained sheets were used for DSC experiments.

A Perkin–Elmer Diamond DSC calibrated with indium and zinc standards was used to monitor nonisothermal crystallization kinetics of the sPS samples, for minimizing thermal lag between the polymer sample and the DSC furnace, the sheets were cut into disk-shaped pieces and the sample weights were 7–8 mg.

For the nonisothermal cold-crystallization, the quenched sPS sample sheets were heated at rates of 2.5, 5, 10, 20, 30, 40, and 60°C/min, respectively. For comparison, isothermal cold-crystallization was carried out as well. The quenched sPS sheets were heated at 200°C/min from 50°C to 130, 134, 136, 140, 144, and 148°C, respectively, and stayed at these temperatures to let the samples crystallize, respectively, while for the nonisothermal melt-crystallization, the sheets were first heated to 320°C, stayed at this temperature for 5 min to eliminate any residual nuclei that might act as seed crystals, and then cooled at different constant rates—5, 10, 20, 30, 40, 60, and 80°C/min, respectively. The relative crystallinity at a definite temperature was calculated by the supplied software of this instrument for further analysis of various macrokinetic models.

Polarized optical microcopy

The morphology of various thin film samples of sPS was observed by using a polarized optical microscope (Leika) equipped with a Linkam-THMSE-600 automatic thermal control hot-stage (with the controlling temperature precision of ±0.1°C), a JVC model digital-color-video camera, a liquid-nitrogen cold-trap, and a computer. The sPS sample was firstly dissolved into *p*-xylene at 140°C with weight concentration of 2%, and then the solution was cast onto the surface of a cover glass placed in a petri dish. After the film was cast, *p*-xylene was then allowed to evaporate in the vacuum oven at 60°C for 1 week. For morphology observation of nonisothermal cold-crystallization, the sPS films were firstly heated to 320°C, and then quenched to ice water; after drying the quenched films under vacuum at room temperature, the films were heated on the POM hot-stage at different rates to observe the crystalline morphology of sPS for parallel comparison with nonisothermal cold-crystallization experiments. After completing the observation of cold-crystallization with a definite heating rate, the same sample film was heated to 320°C, stayed for 5 min, followed by cooling at the same value as that of the heating rate of cold-crystallization process to observe the end-morphology from nonisothermal melt-crystallization for the same rate (heating or cooling).

Wide angle X-ray diffraction

Wide-angle X-ray diffraction (WAXD) experiments were performed at room temperature by using a Rigaku D/max 3C diffractometer with curved graphite crystal-filtered Cu $K\alpha_1$ radiation ($\lambda = 0.15406$ nm). The sheet specimens were fixed on the rotating sample stage of the goniometer to eliminate any anisotropic effects, and so that suitable averages of the diffracted intensities in reciprocal space could be obtained. Data were collected over the range $2\theta = 5$–30° in the fixed time mode with a step interval of 0.02°.

For nonisothermal cold-crystallization, since the maximum end-temperature of the crystallization [see curve of 60°C/min in Fig. 1(a)] for all rates investigated is not more than 200°C, we selected 210°C as the upper stopped temperature. We heated the quenched samples on the POM hot-stage from 50°C at different heating rates (5, 10, 20, 30, and 60°C/min) to 210°C, respectively, stayed at this temperature for 5 min, followed by cooling at 10°C/min to 50°C, and then naturally cooled to room temperature for WAXD experi-

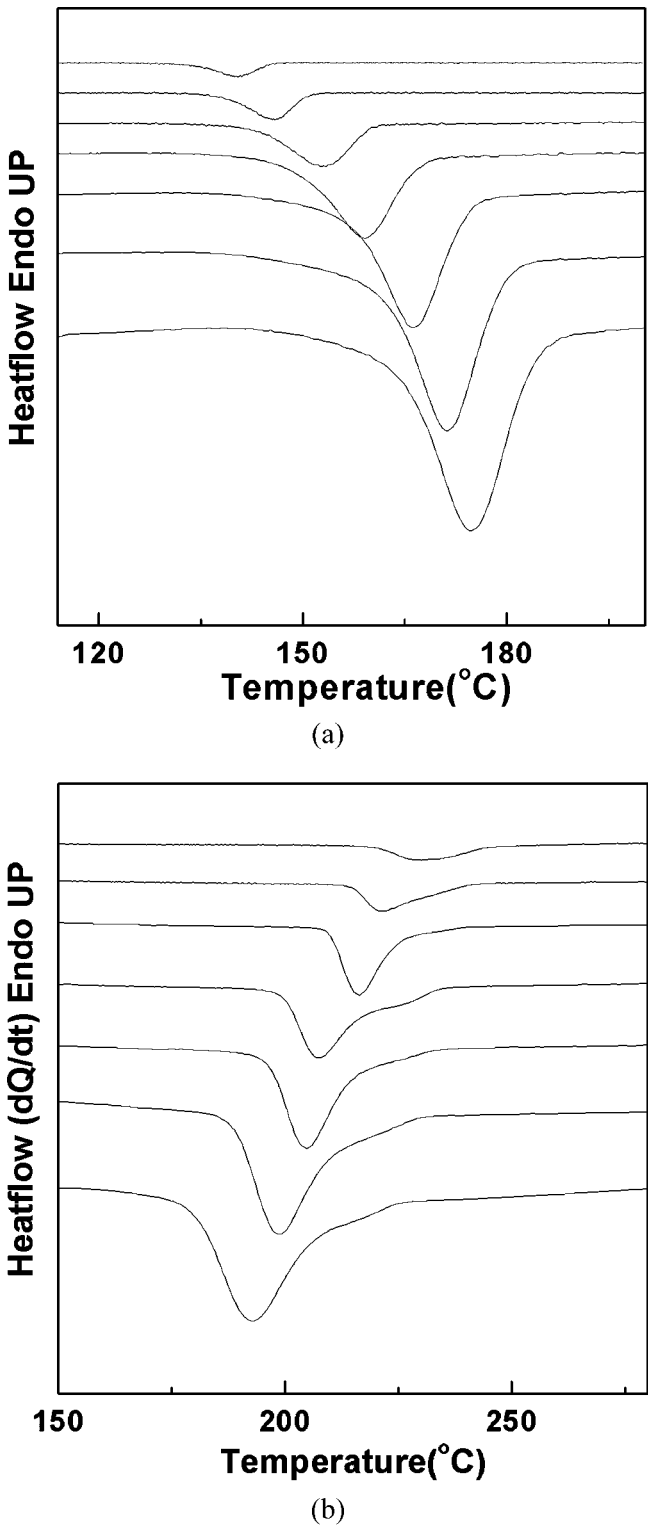

Figure 1 Curves of nonisothermal cold-crystallization (a) and melt-crystallization (b) of sPS at different rates indicated. (a) 2.5, 5, 10, 20, 30, 40, and 60°C/min; (b) 5, 10, 20, 30, 40, 60, and 80°C/min.

ments. For nonisothermal melt-crystallization, the sample sheets were firstly heated at 100°C/min from 50 to 320°C on the POM hot-stage, stayed at this temperature for 5 min, followed by cooling at different cooling rates (5, 10, 20, 30, 60, and 80°C/min) to 50°C, and then naturally cooled to room temperature for WAXD experiments.

RESULTS AND DISCUSSION

Heat flow evolution, morphology, and structures

Figure 1(a) shows nonisothermal cold-crystallization exotherms of sPS for seven different heating rates, ranging from 2.5 to 60°C/min. Clearly a single crystallization exotherm was observed for each heating and the exothermic curve became wider and shifted to a higher temperature with increasing heating rate used, while for nonisothermal melt-crystallization [Fig. 1(b)], the single exotherm was observed to become wider and shift to lower temperature with increasing cooling rate. For simplification, the nonisothermal cold-crystallization process was replaced by ''A'' and nonisothermal melt-crystallization by ''B'' in later section.

In the nonisothermal crystallization study using DSC instrument, the energy released during the crystallization process appears to be a function of temperature rather than time as in the case of isothermal crystallization. In this way, the relative crystallinity function of temperature $X_t(T)$ can be formulated as

$$X_t(T) = \frac{\int_{T_0}^{T} \left(\frac{dH_c}{dT}\right) \cdot dT}{\Delta H_c} \quad (1)$$

where T_0 and T represent the onset and an arbitrary temperature, respectively, dH_c is the enthalpy of crystallization released during an infinitesimal temperature range dT, and ΔH_c is the total enthalpy of crystallization for a specific cooling rate, the normalized total heat of crystallization was collected and summarized in Table I.

It should be noticed that there should exist more or less temperature lag between furnace and the sample for every heating or cooling rate, but it is negligible for lower cooling rate; whereas the temperature correction is beyond the main-thread of the present work except that the temperature correction procedure is complicated and time-consuming.[15] Furthermore, for our present work, we aim at comparing the difference between cold- and melt-crystallization processes for the same rate (with almost the same temperature lag between furnace and the sample for the same sample sheet); in the following section, it will be found that the results from the analysis of experimental data from lower to higher rates indicated the similar difference between cold-crystallization and melt-crystallization processes. Therefore, the temperature data for all rates to be analyzed were processed as received without any correction.

TABLE I
Characteristic Data of Nonisothermal Cold- and Melt-Crystallization Exotherms for sPS

Φ (°C/min)	$T_{0.01}$ (°C)	T_p (°C)	$X_t(T_p)$ (%)	$T_{0.99}$ (°C)	${t_{1/2}}^{-1}$ (min^{-1})	ΔH (J/g)
2.5	126.7	140.6	61.1	147.2	0.17	17.56
	(–)	(–)	(–)	(–)	(–)	(–)
5	132.7	146.0	63.3	154.0	0.35	18.04
	(250.3)	(223.7)	(61.2)	(229.8)	(0.24)	(25.61)
10	135.8	153.1	59.8	162.2	0.54	18.67
	(244.7)	(217.3)	(62.8)	(221.9)	(0.46)	(25.33)
20	139	159.3	59.4	171.9	0.91	19.04
	(240.7)	(212.2)	(60.8)	(216.4)	(0.74)	(25.04)
30	141.2	166.4	59.6	179.2	1.09	18.33
	(236.5)	(202.6)	(63.2)	(207.5)	(1.01)	(25.52)
40	143.6	171.3	59.2	185.8	1.32	17.94
	(234.3)	(198.6)	(61.5)	(204.7)	(1.25)	(26.74)
60	150.2	174.8	58.5	189.5	2.22	18.53
	(229.1)	(191.8)	(62.1)	(198.8)	(1.96)	(25.77)
80	–	–	–	–	–	–
	(223.5)	(183.5)	(60.5)	(193.1)	(2.50)	(26.42)

Data obtained are those from nonisothermal cold-crystallization and those in parentheses are from nonisothermal melt-crystallization.

To obtain the kinetic information, the experimental data such as those shown in Figure 1(a, b) are needed to be converted to the relative crystallinity function of temperature $X_t(T)$. From nonisothermal cold-crystallization curves [Fig. 2(a)], some kinetic data such as $T_{0.01}$ (the temperature at 1% relative crystallinity), T_p (the temperature at the maximum crystallization rate or the peak temperature), $X_t(T_p)$ at the peak temperature, and $T_{0.99}$ (the temperature at 99% relative crystallinity) could be extracted and listed in Table I. For comparison, the data of $T_{0.01}$, T_p, and $T_{0.99}$ from A were also listed in Table I, together with those of B data. Noticeably, for A, $T_{0.01}$, T_p, and $T_{0.99}$ are all transferred to higher temperatures when the heating rate increases, while for B, $T_{0.01}$, T_p, and $T_{0.99}$ are all shifted to lower temperatures when the cooling rate increases. It should be also noted that $T_{0.01}$ and $T_{0.99}$ represent the apparent onset and end temperatures of A and B of the materials, respectively.

To use eq. (1) to analyze nonisothermal crystallization data obtained by DSC, it is assumed that the sample experiences the same thermal history as designated by the DSC furnace. This may be achieved only when the lag between the temperatures of the sample and the furnace is kept minimal. If this assumption is valid, the relation between the crystallization time t and the sample temperature T can be expressed as[16]

$$t = \frac{T_0 - T}{\Phi} \tag{2}$$

where Φ is the cooling rate. According to eq. (2), the temperature axis (abscissa) observed in Figure 2(a, b) could be transformed into the time scale. The results were exhibited in Figure 2(a, b). It is apparent for A or B that the faster the heating or cooling rate, the shorter the time for completion of the crystallization process.

From Figure 2(a, b), the crystallization time at relative crystallinity $X_t = 0.5$, $t_{1/2}$, can be picked up from the curves. The inverse of $t_{1/2}$ data, $t_{1/2}^{-1}$, are collected and summarized in Table I; it indicates that ${t_{1/2}}^{-1}$ increases with increasing heating or cooling rate and for the same rate the $t_{1/2}^{-1}$ for A is always larger than that for B. Similarly, the crystallization time at an arbitrary relative crystallinity [$t(X_t)$] can be picked up from Figure 2(a, b). The $t(X_t)$ values for different relative crystallinities X_t (i.e., 0.01, 0.1, 0.3, 0.6, 0.9, 0.99) are plotted as a function of heating or cooling rate in Figure 3(a, b). The $t_{0.01}$ and $t_{0.99}$ are the qualitative measures of the beginning and the end of the crystallization process. From the values of $t_{0.01}$ and $t_{0.99}$, the apparent total crystallization period Δt_c can be calculated ($\Delta t = t_{0.99} - t_{0.01}$) and the variations of log Δt_c with heating or cooling rate are plotted in the inserted graph of Figure 3(a, b) as well. The fact that the $t(X_t)$ value for a specific relative crystallinity and the Δt_c value are all found to decrease with increasing heating or cooling rate suggests that nonisothermal crystallization processes proceed faster with increasing heating or cooling rate.

For further analyzing the results obtained, plots of log Δt versus log Φ [the inserted figures in Fig. 3(a, b)] and of log $t(X_t)$ versus log Φ [Fig. 4(a, b)] indicate that these plots exhibit linear relationship, furthermore, all of the plots exhibit similar slope, with average value of -0.793 ± 0.009 $min^2/°C$ for A and -0.764 ± 0.038 $min^2/°C$ for B, while the dependence of logarithm of apparent total crystallization period on logarithm of rate gives intercept and slope being 1.22, −0.757 for A and 1.41, −0.834 for B, respectively.

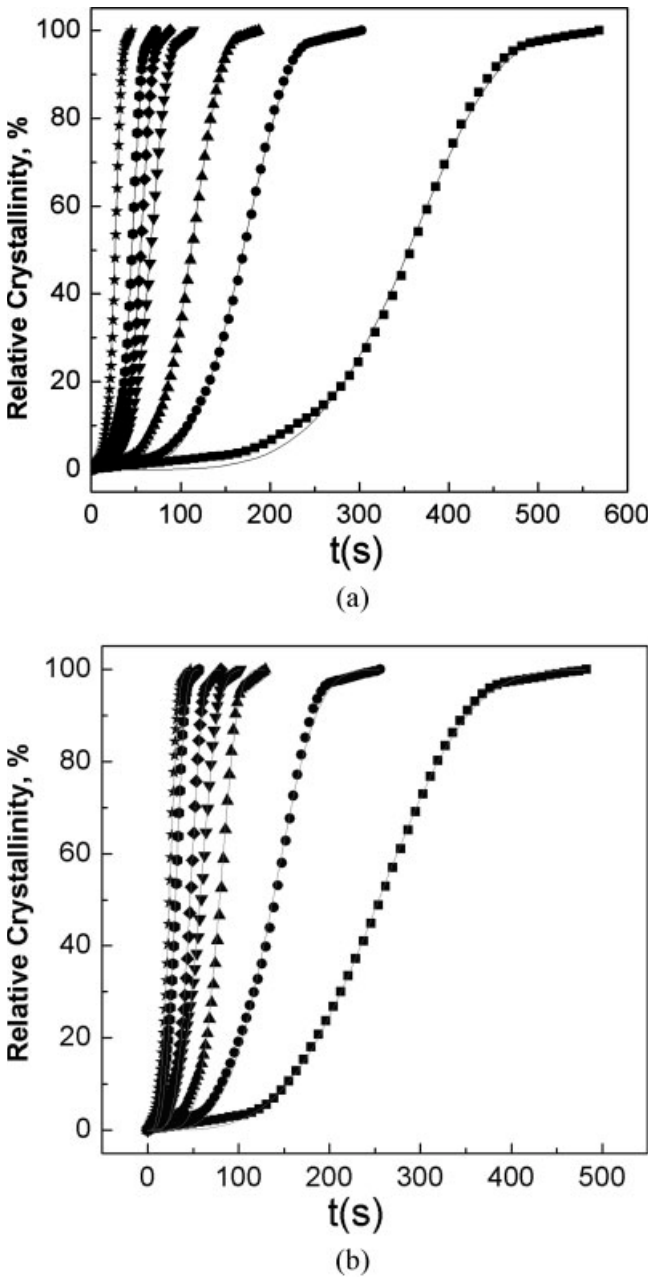

Figure 2 Development of relative crystallinity with crystallization time during nonisothermal cold-crystallization (a) and melt-crystallization (b) of sPS. The solid lines are fitting ones from Tobin equation. (a) 2.5, 5, 10, 20, 30, 40 and 60°C/min, the rate increases according to the sequence of curves from right to left side; (b) 5, 10, 20, 30, 40, 60, and 80°C/min, the rate increases according to the sequence of curves from the right to left side.

For contrasting the morphology of sPS under different processings of A and B, a POM with a CCD camera, which could *in situ* record the growth of the spherulites of this polymer at the time interval, was used. For A, during heating the samples, due to appearance of too many nuclei, the crystallization proceeded so quickly that we could not clearly observe the usual Maltese cross spherulitic morphology, while for B, during cooling, the development of the typical spherulitic morphology could be clearly observed. As an example, the same heating and cooling rate of 5°C/min was selected. Figure 4(a, b) give the typical morphologies for A and B, respectively. In addition, for B, on increasing the cooling rate, the sizes of spherulitic

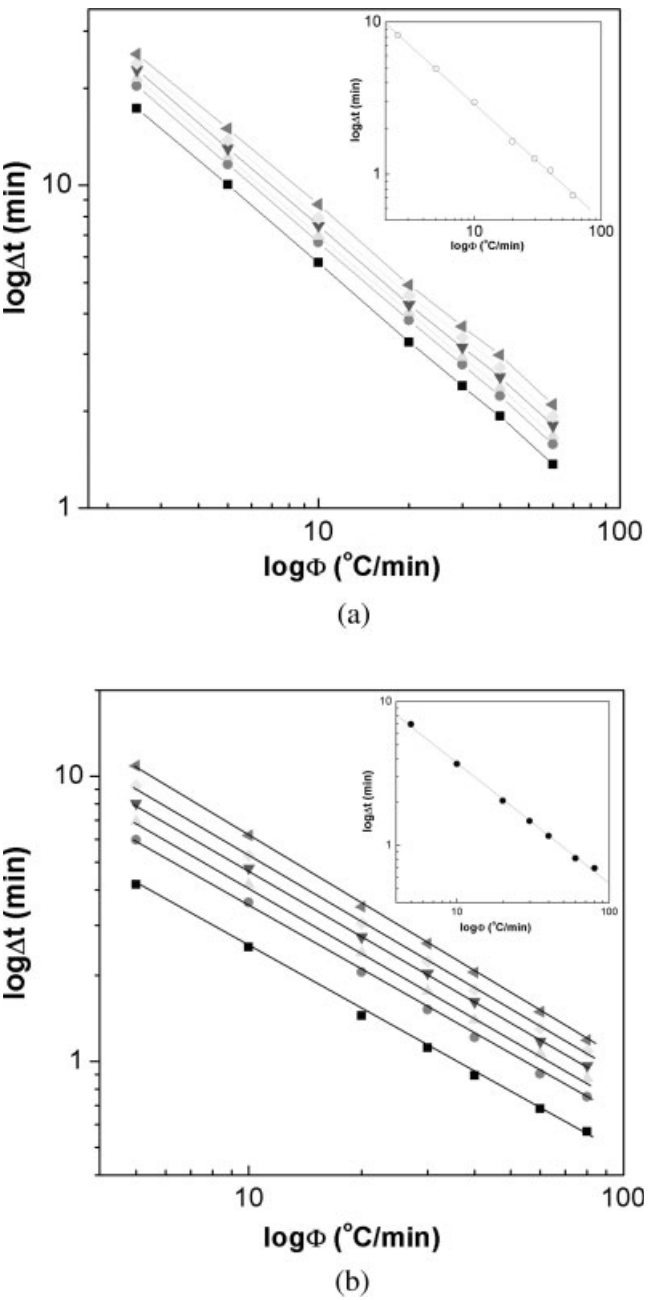

Figure 3 Crystallization time, on nonisothermal cold-crystallization (a) and melt-crystallization (b), of sPS at various relative crystallinity values as a function of cooling rate in log–log plot, respectively. The inset figures in (a) and (b) indicate relationship between apparent total crystallization period and heating or cooling rate in a log–log plot. (a) 0.01, 0.1, 0.3, 0.6, 0.9, 0.99, $\log \Delta t = 1.22 - 0.757 \log \Phi$, $R^2 = 0.9988$; (b) 0.01, 0.1, 0.3, 0.6, 0.9, 0.99, $\log \Delta t = 1.413 - 0.834 \log \Phi$, $R^2 = 0.9985$.

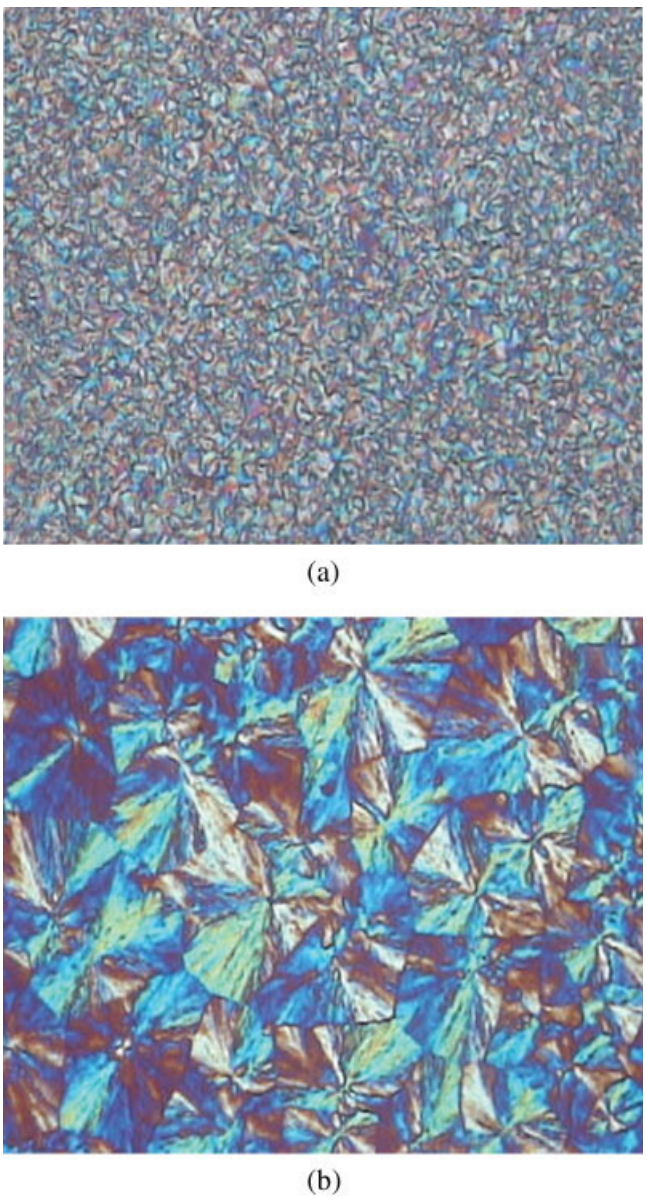

Figure 4 Typical POM morphology obtained by heating at 5°C/min from the quenched samples (a) and cooling at 5°C/min from the melt (b). (a) 50 μm; (b) 50 μm. [Color figure can be viewed in the online issue, which is available at www.interscience.wiley.com.]

morphology in Figure 4(b) become smaller, as is usually expected.

For further investigating the crystal structures of the samples subjected to nonisothermal cold- and melt-crystallization, respectively, X-ray diffraction analysis was carried out. For A, it was found that for all heating rates investigated, the samples contained little crystallinity and did not indicate discernible diffraction peaks, as typically shown in Figure 5(a). The peaks in Figure 5(a) were located at 6.8, 11.8, 13.6, and 20.5°, respectively, which are assigned to a′ crystal according to Guerra et al.[11] At the same time, the shoulder peak appearing at 12.3° means that minor β form crystals existed.[11] It is noteworthy that as we let the quenched sample isothermally crystallized at 180 and 200°C for 2.5 h [for all heating rates, 200°C is above the end-temperature of all cold-crystallization curves in Fig. 1(a)], the X-ray diffractograms (not shown) were still similar to Figure 5(a), indicating that a′ crystal was easily formed below 200°C. As crystallization process was changed from cold-crystallization to melt-crystallization, i.e., the initial state of the amorphous sample varied from rigid glass state to soft melt, X-ray diffraction analysis indicates significant difference between cold- and melt-crystallization [Fig. 5(b)]. A direct observation indicates that the number and sharpness of peaks

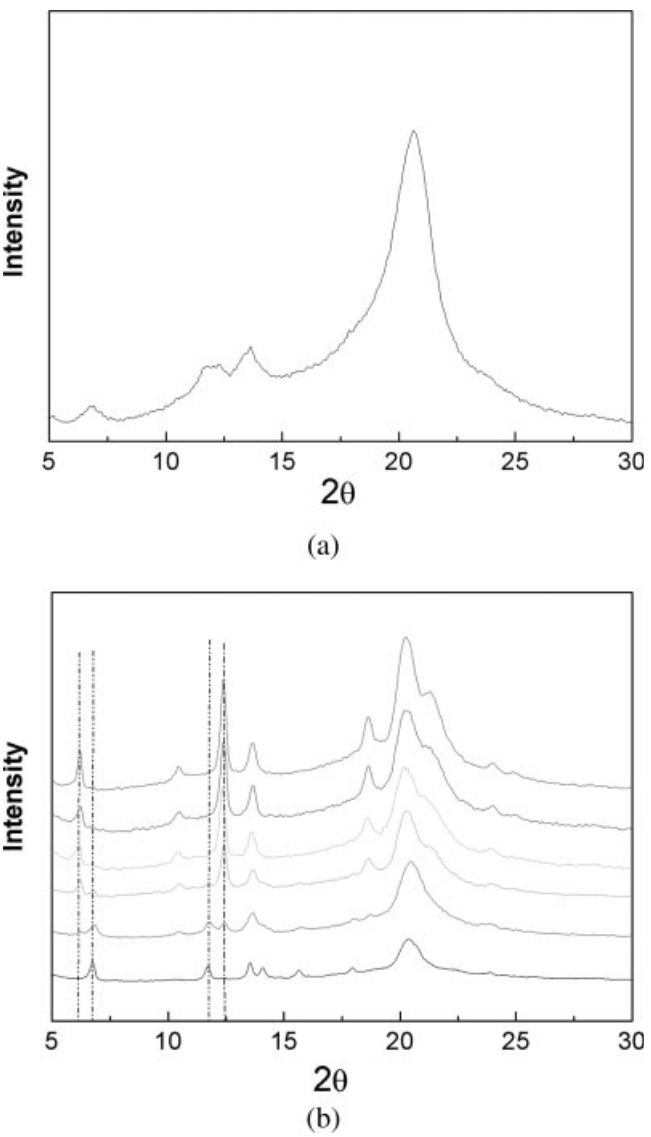

Figure 5 (a) Typical X-ray diffraction pattern of cold-crystallized sPS sample to 210°C; (b) X-ray diffractograms of sPS sample firstly melted at 320°C, followed by cooling at different cooling rates to 50°C, and then naturally cooled to room temperature. The dashed lines indicate the positions of the characteristic peaks of α and β crystals. (a) (110), (300), (200), and (211); (b) (020), (110), (040), (130), (060), (111), (041), (170), (080); 5, 10, 20, 30, 60, and 80°C/min.

of the samples subjected to melt-crystallization differ from those of the cold-crystallization process. As the sample was cooled at 5°C/min from the melt to 50°C and measured at room temperature, peaks appear at positions of 6.2, 10.4, 12.4, 13.6, 18.6, 20.3, 21.3, and 24.0°. According to Guerra et al.,[11] these peaks are assigned to β crystal. The corresponding crystal planes are marked in the corresponding peaks of Figure 5(b). For cooling rate below 20°C/min, only diffraction peaks of β crystal are observed; as cooling rate is above 20°C/min, new peaks characteristic of α-type crystal were observed [which are indicated with dash lines, together with characteristic peaks of β crystal in Fig. 5(b)], the intensity of which increases with increasing cooling rate. As cooling rate reached 80°C/min, it was found that characteristic peaks of β crystal disappear and the peaks appearing at 6.8, 11.8, 13.6, 14.1, 15.7, 18.0, and 20.4° are assigned to α-type crystal,[11] which correspond to (110), (300), (220), (310), (400), (410), and (211) crystal planes, respectively. Obviously the α-type crystal obtained from melt-crystallization is a little different from cold-crystallization, observed were added peaks at 14.1, 15.7, 18.0°, characteristic of α-type crystal.[11] The variation of relative contents of α crystal and β crystal in the formed crystal mixtures with cooling rates is in accordance with the observation of Guerra et al.[4,11] and Li et al.[12]

Chen et al.[17] have suggested the following formulae for calculating crystallinity of α′-, α″-, and β-type crystals through correcting the peaks of weaker intensity into the universal correction factor (the peak corresponding to (110) crystal plane for α′ crystal, the peaks to (110) and (210) crystal planes for α″ crystal, and the peaks to (020) and (170) crystal planes for β crystal were corrected, respectively):

$$W_{\alpha\prime} = \frac{I_{300} + 1.43I_{220} + 4.48I_{211}}{I_{300} + 1.43I_{220} + 4.48I_{211} + 3.44I_a} \times 100\% \quad (3a)$$

$$W_{\alpha''} = \frac{0.70I_{300} + I_{220} + 1.46I_{400} + 2.15I_{410} + 3.15I_{211}}{0.70I_{300} + I_{220} + 1.46I_{400} + 2.15I_{410} + 3.15I_{211} + 2.42I_a} \times 100\% \quad (3b)$$

$$W_{\beta} = \frac{I_{110} + 1.46I_{040} + 1.87I_{130} + 4.27I_{060} + 5.15I_{111} + 6.50I_{041}}{I_{110} + 1.46I_{040} + 1.87I_{130} + 4.27I_{060} + 5.15I_{111} + 6.50I_{041} + 4.46I_a} \times 100\% \quad (3c)$$

The crystallinity of sPS samples subjected to different heating (A) or cooling rate (B) were thus calculated by using eqs. (3a), (3b), or (3c), and listed in Table II. It was found that the crystallinity value for cold-crystallization is always lower than that for melt-crystallization for the same rate.

For comparison purpose, we used the normalized total heat of crystallization, listed in Table I, to be divided by 53.2 J/g, which is the melting enthalpy of 100% crystallinity, as suggested by Paszto et al.[18] The calculated results are indicated in Table II. Table II indicates that the data for A are lower than those for B for the same rate, similar to the results obtained from WAXD technique.

Guerra et al.[11] have suggested a technique to quantitatively estimate the content of α- and β-type crystal forms from WAXD patterns obtained from melt-crystallization. The 2θ range of 10–15° is considered, and a baseline between the two intensity minima located at 2θ = 10.8° and 2θ = 14.8° is drawn. The area (A) of the two peaks located at 2θ = 11.6° and 2θ = 12.2° are measured, and the percent content of the α form in the blend with α- and β-type crystals can be evaluated by the following formula:

$$P_\alpha = \frac{\frac{1.8A(11.6)}{A(12.2)}}{1 + \frac{1.8A(11.6)}{A(12.2)}} \times 100 \quad (4)$$

where 1.8 is the ratio between the intensities (measured in the same experimental conditions) of the peaks at 11.6 and 12.2° for samples of equal thickness and crystallinity in the pure α- and β-type crystal forms, respectively. The percent of α form for cooling rates of 20, 30, 60, and 80°C/min are calculated and listed within parentheses in melt-crystallization column in Table II. The data in Table II indicate that below 20°C/min, only β-type crystal can be observed; for cooling rates of 20 and 30°C/min, minor α form crystal with major β-type crystal exists in the end

TABLE II
Crystallinities Obtained from WAXD and DSC Techniques for Nonisothermal Cold- and Melt-Crysallization of sPS

Rate (°C/min)	Cold-crystallization		Melt-crystallization	
	W (WAXD)	*W* (DSC)	*W* (WAXD)	*W* (DSC)
5	0.403	0.339	0.542	0.481
10	0.407	0.351	0.548	0.476
20	0.393	0.358	0.538 (2.3)[a]	0.471
30	0.411	0.345	0.535 (6.0)	0.480
60	0.414	0.348	0.544 (74.9)	0.484
80	–	–	0.558 (98.6)	0.497

[a] The data in the parentheses indicate the percent ratio of the α″-type crystal form in the blend of α″ and β-type crystal forms of sPS.

materials; while as cooling rate is increased to 60°C/min, α form crystal becomes the major component in the crystal blend; and for more higher cooling rate, such as 80°C/min, the whole material was basically inhibited by α form crystal.

Kinetic analysis of cold and melt nonisothermal crystallization

Modified Avrami analysis

Avrami equation[19,20] is the most popular equation to describe the overall isothermal crystallization process of polymers and has the expression as follows:

$$X_t = 1 - \exp[-K_A \cdot t^{n_A}] \in [0,1] \quad (5)$$

where the parameter K_A is a composite rate constant involving both nucleation and growth rate parameters. The exponent n_A is a constant, which describes the crystallization mechanism and bears relation to nucleation type and growth process. It should be noted that the units of K_A are given as an inverse of time. Mandelkern[21] thought that the primary stage of nonisothermal crystallization could be described by Avrami equation, which is based on the assumption that T_c is constant. i.e.

$$X_t = 1 - \exp[-Z_t \cdot t^{n_A}] \in [0,1] \quad (6)$$

or

$$\log(-\ln(1 - X_t)) = \log Z_t + n_A \log t \quad (7)$$

where Z_t is the rate constant in the nonisothermal crystallization process. Jeziorny[16] believed that the Z_t in eqs. (6) and (7) should be related to heating or cooling rate, Φ. Presuming the constant Φ, the final form of characterizing the kinetics of nonisothermal crystallization was given by

$$\log Z_c = \frac{\log Z_t}{\Phi} \quad (8)$$

By linear regression technique on data in the primary stage of plots of log [−ln (1 − X_t)] versus log t in eq. (7), we could easily obtain the Avrami exponent and rate constant Z_t or Z_c from the slope and the intercept. The values are listed in Table III. For A, the Avrami exponent n_A ranges from 3.3 to 2.2, and the rate constants Z_t and Z_c increase with increasing heating rate. For B, the Avrami exponent n_A ranges from 3.7 to 2.7, the rate constants Z_t and Z_c increase with increasing cooling rate as well. Comparing the Avrami exponent n_A of A and B, it was found that for the same rate (heating and cooling), the n_A for A is always less than that for B and the rate constants Z_t and Z_c for A are larger than those for B for the same rate, respectively. The Avrami exponents in Table III mean that during nonisothermal crystallization processes of sPS, the possible mechanisms are three dimensional spherulite growth with thermal nucleation for lower rates and athermal nucleation, followed by two (for A) or three (for B) dimensional spherulite growth for higher rates.[21]

TABLE III
Parameters of Nonisothermal Cold- and Melt-Crystallization Kinetics for sPS, Obtained from Modified Avrami Analysis

Φ	Cold-crystallization			Melt-crystallization		
(°C/min)	n	log Z_t	log Z_c	n	log Z_t	log Z_c
2.5	3.3	−8.94	−3.58	–	–	–
5	2.8	−8.30	−1.66	3.7	−9.14	−1.83
10	2.2	−6.04	−0.60	3.7	−8.01	−0.80
20	2.3	−5.44	−0.27	2.7	−5.61	−0.28
30	2.4	−5.07	−0.17	2.8	−5.22	−0.17
40	2.5	−4.19	−0.10	2.8	−4.96	−0.12
60	2.2	−4.0	−0.067	2.8	−4.38	−0.073
80	–	–	–	2.9	−4.20	−0.052

Tobin analysis

In the original derivation of the Avrami model, the effects of growth site impingement and secondary crystallization process were neglected for the purpose of simplicity, which results in that the Avrami approach model is only suitable for describing the early stages of crystallization. Tobin proposed a theory for phase transformation kinetics with consideration of growth site impingement.[22–24] According to this approach, the relative crystallinity function of time X_t can be expressed in the following form:

$$X_t = 1 - \frac{1}{1 + (K_T \cdot t)^{n_t}} \in [0,1] \quad (9)$$

where K_T and n_T are the Tobin crystallization rate constant and the Tobin exponent, respectively. On the basis of this proposition, n_T need not be an integer[24] and is also governed by different types of nucleation and growth mechanisms. Fitting the data with different rates in Figure 2(a, b) to eq. (9) the Tobin kinetic parameters K_T and n_T, together with the R^2 parameters, were obtained from the best fits. The fitting lines are indicated in Figure 2(a, b) as solid lines. These parameters are listed in Table III. The Tobin exponents n_T for A and for B were found to range from 2.6 to 3.5 and 2.9 to 3.9, respectively, while whether for A or B, the Tobin crystallization rate constant K_T was found to increase with increasing heating or cooling rate. When comparing the Tobin exponent n_T and rate constant K_T of A and B, the same trend as Avrami exponent and rate constants above was observed, i.e., the n_T for A is less than that for B and the rate constant K_T for A is larger than that for B for the same rate. Comparing the Avrami parameters n_A in Table III and Tobin

TABLE IV
Parameters of Nonisothermal Cold- and Melt-Crystallization Kinetics for sPS, Obtained from Tobin Analysis

Φ	Cold-crystallization			Melt-crystallization		
(°C/min)	n_T	log K_T	R^2	n_T	log K_T	R^2
2.5	3.4	−9.06	0.99871	–	–	–
5	3.5	−8.26	0.99795	3.9	−10.40	0.99889
10	3.3	−7.05	0.9993	3.7	−8.07	0.99989
20	2.8	−5.95	0.99571	3.0	−6.14	0.99748
30	2.9	−5.43	0.99927	3.1	−5.67	0.99949
40	2.7	−4.89	0.99911	3.0	−5.27	0.99635
60	2.6	−4.19	0.99756	2.9	−4.48	0.99704
80	–	–	–	2.9	−4.20	0.99635

exponent n_T in Table IV, it was found that whether A or B, n_T is always larger than n_A for the same heating or cooling rate. The Tobin exponents n_T should have the same physical meaning as the Avrami exponent, i.e., during nonisothermal crystallization processings, the possible mechanisms are three dimensional spherulite growth with thermal nucleation for lower rates and athermal nucleation, followed by two or three dimensional spherulite growth for higher rates.[21]

Ziabicki's kinetic crystallizability analysis

Ziabicki[25–27] suggested that the kinetics of polymeric phase transformation could be described to be a first-order kinetic equation as:

$$\frac{dX_t}{dt} = K_\Phi(T) \cdot (1 - X_t) \tag{10}$$

where $K_\Phi(T)$ is a crystallization rate function with a temperature-dependence. In the case of nonisothermal crystallization, both X_t and $K_\Phi(T)$ vary and are dependent on the heating or cooling rate Φ. For a definite rate, the crystallization rate function $K_\Phi(T)$ can be expressed by a Gaussian function:

$$K_\Phi(T) = K_{\Phi,\max} \cdot \exp\left[-\frac{2.773(T - T_{\max})^2}{D_\Phi^2}\right] \tag{11}$$

where $T_{\max}$ is the temperature at which the crystallization rate is maximum, $K_{\Phi,\max}$ is the maximum crystallization rate at $T_{\max}$, and D_Φ is the width at half-height determined from the crystallization rate function. Using the isokinetic approximation, integration of eq. (11) over the whole crystallizable range (i.e., $T_g < T < T_m^o$) leads to an important characteristic value describing the crystallization ability of a semicrystalline polymer, i.e., the kinetic crystallizability index G_Φ:

$$G_\Phi = \int_{T_g}^{T_m^o} K_\Phi(T)dT \approx 1.064 \cdot K_{\Phi,\max} \cdot D_\Phi \tag{12}$$

In the case of nonisothermal crystallization studies using DSC, $K_{\Phi,\max}$ in eq. (12) is the maximum crystallization rate for each definite rate studied and is expressed as:

$$K_{\Phi,\max} = \frac{C_k}{T_{\max}} \tag{13a}$$

where

$$C_k = \frac{\int_0^{t_{\max}} \left(\frac{dH}{dt}\right) \cdot dt}{\int_{t\max}^{\infty} \left(\frac{dH}{dt}\right) \cdot dt} \tag{13b}$$

$t_{\max}$ in eqs. (13a) and (13b) is the time from the beginning of crystallization to reach the maximum crystallization rate for each cooling rate.[16]

According to eqs. (13a) and (13b), G_Φ is the kinetic crystallizability index for an arbitrary rate. The Ziabicki kinetic crystallizability index G, considering the effect of cooling rate, can therefore be obtained by normalizing G_Φ with Φ

$$G = \frac{G_\Phi}{\Phi} \tag{14}$$

as first suggested by Jeziorny.[16]

According to Jeziorny's approach above,[16] the parameters $K_{\Phi,\max}$, D_Φ, G_Φ for A were calculated and listed in Table V, respectively. Table V indicates that $T_{\max}$, Φ, $K_{\Phi,\max}$, D_Φ, and G_Φ increase with increase of heating rate. After normalizing G_Φ with the heating rate using eq. (14), the value of the kinetic crystallizability at unit cooling rate, G can be determined and the data are summarized in Table IV, which indicates that the normalized G values obtained for different heating rates were almost identical, with the average value being 1.28. According to the same procedure above, the parameters $K_{\Phi,\max}$, D_Φ, G_Φ, and G for B were calculated and summarized in Table VI. Table VI indicates that $T_{\max}$ decrease, while $K_{\Phi,\max}$, D_Φ, and G_Φ increase with increasing cooling rate, the obtained G were almost identical with the average value being 1.07. It is noteworthy that for a same polymer, two G

TABLE V
Parameters Obtained from Ziabicki's Kinetic Crystallizability Analysis on Nonisothermal Cold-Crystallization Kinetics for sPS

Φ	$T_{\max,\Phi}$	D_Φ		$G_{Z,\Phi}$	
(°C/min)	(°C)	(°C)	$K_{\Phi,\max}$	(°C/min)	G_Z
2.5	140.6	6.78	0.45	3.24	1.30
5	146.0	7.24	0.78	6.03	1.21
10	153.1	9.81	1.27	13.29	1.33
20	159.3	10.77	2.22	25.41	1.27
30	166.4	11.53	3.12	38.33	1.28
40	171.3	12.22	3.73	48.46	1.21
60	174.8	12.64	6.05	81.34	1.36

TABLE VI
Parameters Obtained from Ziabicki's Kinetic Crystallizability Analysis on Nonisothermal Melt-Crystallization Kinetics for sPS

Φ (°C/min)	$T_{max,\Phi}$ (°C)	D_Φ (°C)	$K_{\Phi,max}$	$G_{Z,\Phi}$ (°C/min)	G_Z
5	229.8	14.19	0.35	5.27	1.05
10	222.0	15.51	0.67	11.01	1.10
20	216.5	16.59	1.23	21.63	1.08
30	207.5	16.71	1.74	30.94	1.03
40	204.7	17.73	2.17	40.87	1.02
60	198.9	18.95	3.23	65.07	1.08
80	193.1	20.45	4.07	88.48	1.11

values are obtained, the difference of the G values obtained from cold- and melt-crystallization, respectively, is possibly due to the reason that there exists partially ordered structures formed during quenching in the quenched samples, which acted as self-seeded nuclei during cold-crystallization and changing the crystallization process, resulting in reduced Avrami exponent and Tobin exponent and improved crystallization rate, as indicated above.

Combination with Avrami and Ozawa equation

On the basis of the mathematical derivation of Evans,[28] Ozawa extended the Avrami theory to describe the nonisothermal crystallization case by assuming that the sample was cooled with a constant rate.[29] In the Ozawa method, the time variable in the Avrami equation was replaced by a cooling rate and the relative crystallinity was derived as a function of constant cooling rate as

$$X_t = 1 - \exp\left[-\frac{K_0}{\Phi} n_0\right] \tag{15}$$

or

$$\log[-\ln(1 - X_t)] = n_0 \log K_0 - n_0 \log \Phi \tag{16}$$

where K_0 and n_0 are the Ozawa crystallization rate constant and the Ozawa exponent, respectively. Both of the Ozawa kinetic parameters (i.e., K_0 and n_0) hold similar physical meanings to those of the Avrami ones (i.e., K_A and n_A). Drawing the plots of log [−ln (1 − X_t)] versus log Φ for a fixed temperature, straight lines should be obtained, but we did not. The experimental facts indicate that the Ozawa equation could not well describe the nonisothermal crystallization process of sPS. Mo and coworkers[30–32] suggested an equation by combining the Avrami and Ozawa equations. It has successfully described the nonisothermal crystallization process of several samples such as Nylon66, Nylon11, PEDEKK, etc. as follows:

$$\log \Phi = \log F(T) - a \log t \tag{17}$$

where $a = n_A/n_0$, i.e., the ratio of the Avrami exponent to the Ozawa exponent; the parameter $F(T)$ refers to the value of the cooling rate, which has to be chosen at unit crystallization time when the measured system amounts to a certain degree of crystallinity.

According to eq. (17), the plots of log Φ versus log t at definite relative crystallinities (0.1, 0.3, 0.6, 0.9) are presented in Figure 6(a, b). Good linear relationships between log Φ and log t were exhibited. The a, $F(T)$,

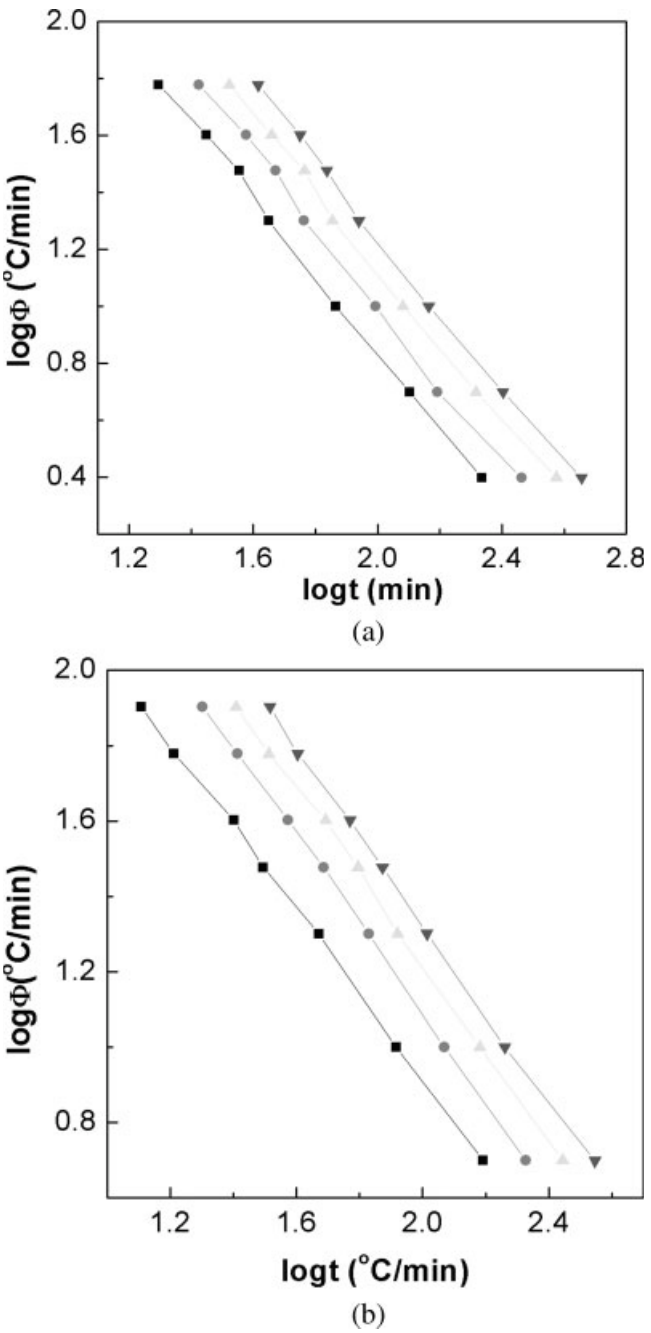

Figure 6 Plots of log Φ versus log t for a definite relative crystallinity for nonisothermal cold-crystallization (a) and melt-crystallization (b). (a) 0.1, 0.3, 0.6, 0.9 the relative crystallinity increases according to sequence of the curves from the left to right side.

TABLE VII
Parameters log $F(T)$, a, and R^2-Correlation Coefficients, Obtained from Combination of Ozawa and Avrami Equations for Nonisothermal Cold- and Melt-Crystallization of sPS

Relative crystallinity	a	log $F(T)$	R^2
0.1	1.4	3.55	0.9983
	(1.1)	(3.14)	(0.9990)
0.3	1.4	3.74	0.9971
	(1.2)	(3.45)	(0.9993)
0.6	1.3	3.80	0.9976
	(1.2)	(3.56)	(0.9988)
0.9	1.3	3.93	0.9979
	(1.2)	(3.67)	(0.9992)

Data obtained are those from nonisothermal cold-crystallization and those in parentheses are from nonisothermal melt-crystallization.

and R^2-correlation coefficients are obtained by least square method and listed in Table VII. It is clear that a is almost a constant, being 1.3–1.4 for A and 1.1–1.2 for B, and $F(T)$ increases with increasing crystallinity, suggesting that the higher the relative crystallinity, the higher the heating or cooling rate needed for A and B, respectively.

Effective energy barrier

The Avrami, Tobin, Ozawa, and the combination of Avrami and ozawa analysis do not propose a technique for estimating the effective energy barrier for nonisothermal crystallization process, ΔE. Kissinger[33] has suggested an expression for evaluating the effective energy barrier ΔE, which have correlated the scanning rate Φ with the peak temperature T_p obtained for a given condensed phase transformation as follows:

$$\frac{d\ \ln(\Phi/T_p^2)}{d(\frac{1}{T_p})} = -\frac{\Delta E}{R} \tag{18}$$

where T_p is the peak temperature of nonisothermal cold- or melt-crystallization curves and ΔE is the activation energy corresponding to nonisothermal cold- or melt-crystallization. It is noteworthy that Vyazovkin have suggested that Kissinger equation is not applicable to nonisothermal melt-crystallization process (B) for the reason that eq. (18) does not permit substitution of negative heating rates (cooling rates),[34,35] while for nonisothermal cold-crystallization process (A), Kissinger should be effective for not having the sign problem of rates, as suggested by Vyazovkin.[35] The Kissinger plot for A was drawn in Figure 7 and the linear regression yields activation energy of 118 kJ/mol with correlation coefficient of −0.99261.

For a process that occurs on heating such as nonisothermal cold-crystallization, or cooling such as nonisothermal melt-crystallization of polymers, reliable value of effective energy barrier can be obtained by the integral isoconversional method proposed by Vyazovkin[35] and the differential isoconversional method proposed by Friedman.[36] Because of the simplicity and reliability of Friedman's method, it will be used in this work. The Friedman equation is expressed as[37]:

$$\ln\left(\frac{dX_t}{dt}\right)_{X_t} = A - \frac{\Delta E_{Xt}}{R \cdot T} \tag{19}$$

where $(dX_t/dt)_{X_t}$ is the instantaneous crystallization rate function of time at a given relative crystallinity X_t, A is an arbitrary pre-exponential parameter, and ΔE_{X_t} is the effective energy barrier of the process for a given relative crystallinity X_t. By plotting $\ln(dX_t/dt)_{X_t}$ at different cooling rates versus the corresponding reciprocal temperature for a definite X_t, the effective energy barrier ΔE_{X_t} for the nonisothermal crystallization process can be easily estimated from the slope of the plot by minus slope multiplying R. As an example of description, we selected nonisothermal cold-crystallization as an example, the plot, for nonisothermal cold-crystallization, of $\ln(dX_t/dt)_{X_t}$ versus $1/T$ at $X_t = 0.5$ is shown in Figure 8. Figure 8 exhibits good linear relationship, meaning that Friedman equation can be well applicable to calculation of effective energy barrier of nonisothermal cold-crystallization. By linear regression, the ΔE_{X_t} values could be obtained. The ΔE_{X_t} data for different relative crystallinity X_t, ranging from 0.1 to 0.90 with 0.1 increment, were obtained and summarized in Table VIII. The ΔE_{X_t} for A was found to decrease with increasing relative crystallinity from

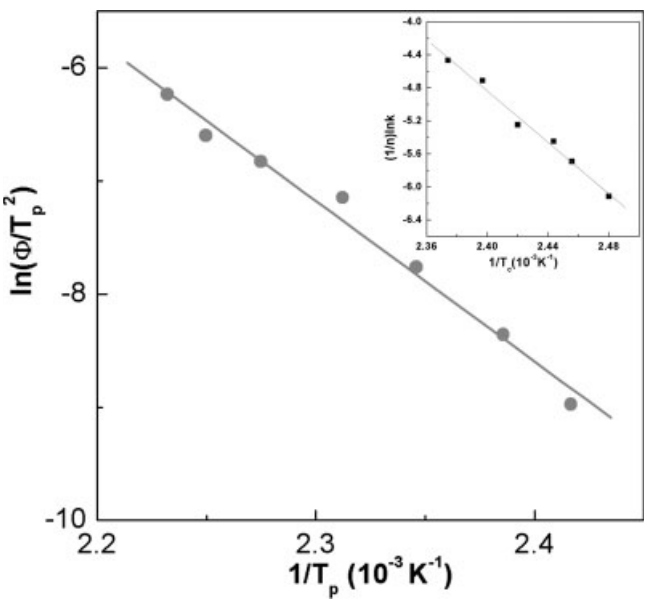

Figure 7 Kissinger plot for evaluating activation energy of nonisothermal cold-crystallization of sPS. The inserted graph is the Arrhenius plot for isothermal cold-crystallization.

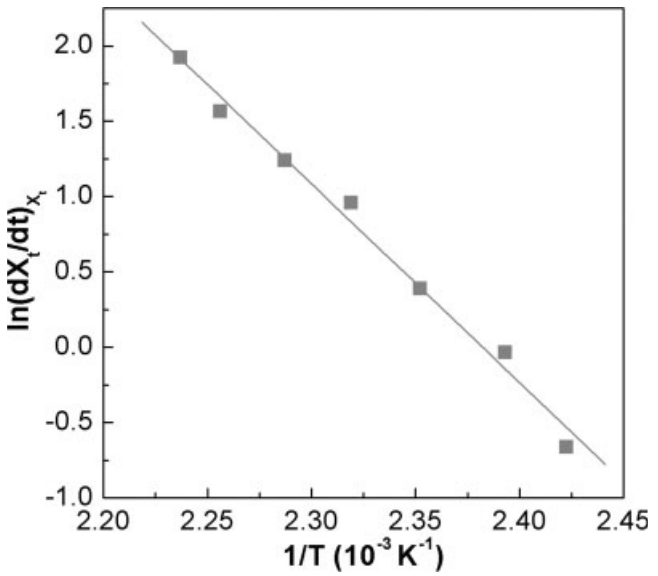

Figure 8 Typical plot for evaluating effective energy barrier using Friedman equation. The relative crystallinity X_t is 0.5.

113.4 kJ/mol at $X_t = 0.1$ to 89.5 kJ/mol at $X_t = 0.90$. Comparing the ΔEs obtained from Kissinger and Friedman equations, respectively, good agreement was observed, indicating Kissinger and Friedman equations could be successfully utilized for calculation of effective energy barrier of nonisothermal cold-crystallization process of sPS. The effective energy barrier values for A in Table VIII are very close to that (148.6 kJ/mol) of a sPS sample with syndiotactity of 90%, obtained by Lu and Nutt[38] using Kissinger equation.

For further examining the cold-crystallization process, isothermal cold-crystallization was also carried out. The temperatures of cold-crystallization were 130, 134, 136, 140, 144, and 148°C, respectively. By Avrami equation analysis, Avrami exponent and the logarithm of rate constant log k are 1.3, 1.5, 1.5, 1.6, 1.7, 2.0; −3.32, −3.61, −3.55, −3.67, −3.52, −3.88 for a definite crystallization temperature. The lower Avrami exponent indicates that the crystallization process of cold-crystallization is different from melt-crystallization. By the well-known Arrhenius equation[34] indicated as follows,

$$k^{\frac{1}{n_A}} = k_0 \cdot \exp\left(-\frac{\Delta E}{R \cdot T_c}\right) \tag{20}$$

$$\frac{1}{n}\ln k = \ln k_0 - \frac{\Delta E}{R \cdot T_C} \tag{21}$$

where k_0 is a temperature independent pre-exponent factor, R is the universal gas constant, ΔE could be obtained by the slope by linear regression on plot of $1/n \ln k$ versus $1/T_c$ (see the inserted graph of Fig. 7) with the value being 130 kJ/mol and correlation coefficient of −0.994. The agreement of the activation energy value obtained by Kissinger and Friedman equations from nonisothermal cold-crystallization and that obtained by Arrhenius equation from isothermal cold-crystallization, respectively, indicate that Kis-

TABLE VIII
Effective Energy Barrier Describing the Overall Nonisothermal Cold- and Melt-Crystallization of sPS, Obtained from the Differential Isothermal Conversional Method of Friedman

Relative crystallinity	ΔE (kJ/mol)	R	ΔE-Group1[a] (kJ/mol)	ΔE-Group2[b] (kJ/mol)
0.1	113.4	−0.96667		
	(−125.1)	(0.97462)	−173.0	−93.1
0.2	112.9	−0.98326		
	(−129.9)	(0.97432)	−217.0	−117.2
0.3	111.6	−0.99062		
	(−129.2)	(0.96145)	−217.0	−117.6
0.4	110.8	−0.99464		
	(−130.4)	(0.96975)	−234.5	−104.5
0.5	109.6	−0.99464		
	(−127.3)	(0.97665)	−257.5	−91.3
0.6	107.6	−0.99621		
	(−127.3)	(0.96878)	−270.9	−82.3
0.7	106.0	−0.99611		
	(−123.8)	(0.97508)	−263.0	−76.5
0.8	102.9	−0.99342		
	(−126.0)	(0.9623)	−267.8	−75.2
0.9	89.5	−0.99565		
	(−125.0)	(0.9823)	−256.2	−78.2

Data obtained are those from nonisothermal cold-crystallization and those in parentheses are from nonisothermal melt-crystallization.
[a] Effective energy barrier obtained from cooling rate below 20°C/min.
[b] Effective energy barrier obtained from cooling rate above 20°C/min.

singer and Friedman equations could well be applied to obtain activation energy from A of sPS.

As such, the effective energy barrier of nonisothermal melt-crystallization of sPS could be obtained using Friedman equation, the results were listed in Table VII, together with the nonisothermal cold-crystallization. The effective energy barrier of nonisothermal melt-crystallization process of sPS ranged from −123.8 to 129.9 kJ/mol, which is smaller than the literature value (−315.9 kJ/mol) obtained by using Kissinger equation[38] (possibly their value is invalid, as suggested by Vyazovkin[35]).

The above structural analysis on WAXD data of sPS samples subjected to melt-crystallization shows that there exists two competitive crystallization processes. For cooling rate below 20°C/min, only β-type crystal crystallization process is observed, while above 20°C/min, the blends of α-type and β-type crystal are formed. In other words, at higher temperature range close to the melting point of sPS, β-type crystal formation was favored, while, at lower temperature, the formation of α-type crystal was preferred.[39,40] Therefore, it is meaningful to divide our melt-crystallization experimental data into two groups, one group includes experimental data for cooling rate below 20°C/min i.e., those for 5, 10, and 20°C/min with only β-type crystal formation; while the other group includes those for cooling rate above 20°C/min, i.e., those for 30, 40, 60, and 80°C/min with both α-type and β-type crystals formation. We reevaluated the two groups of data according to eq. (19) and the obtained effective energy barrier (ΔE) are collected in Table VIII. Table VIII indicates that for group 1, ΔE ranges from −270.9 kJ/mol to −173.0 kJ/mol, decreasing with increasing crystallinity in crystallinity range between 0.1 and 0.7, and then becoming level off as continuing to increase crystallinity; while for group 2, it is a little different from group 1, ΔE first decreases with increasing crystallinity in range between 0.1 and 0.3, and then increases with increasing crystallinity in range between 0.3 and 0.7, as crystallinity is above 0.7, ΔE again becomes level off. In addition, the ΔE values from group 1 is smaller than those from group 2 and from all cooling rates, and the ΔE value from all cooling rates mediate, moreover, the changing range of ΔE, obtained from all cooling rates, with crystallinity becomes less relative to those of groups 1 and 2. The difference of ΔE value between groups 1 and 2 in Table VIII obviously reflects the disparity between the formation of β-type and α-type crystals during nonisothermal melt-crystallization processes.

CONCLUSIONS

The experimental data of nonisothermal cold- and melt-crystallization, for different heating and cooling rates, were obtained from differential scanning calorimetry (DSC) and were thoroughly analyzed based on Avrami, Tobin, Ziabicki, and the combination of Avrami and Ozawa models. The nonisothermal crystallization exotherms of sPS showed that, the temperature at 0.01 relative crystallinity, the peak temperature, and the temperature at 0.99 relative crystallinity transferred to higher temperatures with increasing heating rate for nonisothermal cold-crystallization, but shifted to lower temperatures with increasing cooling rate. This means that increasing heating (cooling) rate will take shorter time to complete cold-(melt-) crystallization. Further data analysis indicated that the apparent induction period, the crystallization time at different relative crystallinity, and the apparent total crystallization period decreased with increasing cooling rate. Both the crystallization time at different relative crystallinity values and the apparent total crystallization period indicated a linear relationship with the heating (or cooling) rate in the log–log plots, with an average slope of -0.793 min^2/°C for nonisothermal cold-crystallization and -0.764 min^2/°C for nonisothermal melt-crystallization.

Avrami, Tobin, and Ziabicki kinetic crystallizability analyses indicate that nonisothermal cold-crystallization process is little different from nonisothermal melt-crystallization; nonisothermal cold-crystallization characterizes smaller Avrami and Tobin exponents and larger kinetic crystallizability index G than those obtained from nonisothermal melt-crystallization. The combination of Avrami and Ozawa equations was found to well describe the experimental data, with exponent a being 1.3–1.4 for nonisothermal cold-crystallization and 1.1–1.2 for nonisothermal melt-crystallization, and the parameter $F(T)$ increasing with increasing relative crystallinity. The effective energy barrier describing the nonisothermal cold-crystallization process of sPS was estimated on the basis of Kissinger equation and the differential isoconversional method of Friedman, respectively; the values obtained by the two equations, respectively, indicate good agreement, furthermore, the activation energy obtained by analyzing the data of isothermal cold-crystallization using Arrhenius equation indicate good accordance with those obtained from Kissinger and Friedman equation, indicating that Kissinger and Friedman equations can be used to obtain activation energy from nonisothermal cold-crystallization analysis of sPS. The effective energy barrier of nonisothermal melt-crystallization was estimated by Friedman's method as well.

WAXD experiments indicate that cold-crystallization mainly obtained α-type crystal but melt-crystallization produced α-type and β-type crystals, the relative content of the crystals in the samples varies with cooling rate and the contents of α-type and β-type crystals with cooling rate were quantitatively evaluated. At lower cooling rate β-type dominates and at

higher cooling rate above 60°C/min, α-type dominates. The experimental data were divided into two groups according to cooling rate and the differential isoconversional method of Friedman was applied to analyze the two group data; it was found that the formation of β-type crystal possesses larger absolute value of effective activation barrier than the formation of α-type crystal. At the same time, POM observation indicates the distinct morphology difference between cold- and melt-crystallization for the same sample film and same rate.

References

1. Ishihara, N.; Shanks, R. A.; Kuramot, M.; Uoi, M. Macromolecules 1989, 19, 2464.
2. Woo, E. M.; Sun, Y. S.; Yang, C. P. Prog Polym Sci 2001, 26, 945.
3. De Rosa, C.; Guerra, G.; Petraccone, V.; Corradini, P. Polym J 1991, 23, 1435.
4. De Rosa, C.; Rapacciuolo, M.; Guerra, G.; Petraccone, V.; Corradini, P. Polymer 1992, 33, 1423.
5. Chatani, Y.; Shimane, Y.; Ijitsu, T.; Yukinari, T. Polymer 1993, 34, 1625.
6. Cimmino, S.; Pace, E. D.; Martuscelli, E.; Corradini, P. Polymer 1991, 32, 1080.
7. Wesson, R. D. Polym Eng Sci 1994, 34, 1157.
8. Hoffman, J. D.; Miller, R. L. Polymer 1997, 38, 3151.
9. Graessley, W. W. J Polym Sci Polym Phys Ed 1980, 18, 27.
10. Woo, E. M.; Sun, Y. S.; Lee, M. L. Polym Commun 1999, 40, 4425.
11. Guerra, G.; Vitagliano, V. M.; De Rosa, C.; Petraccone, V.; Corradini, P. Macromolecules 1990, 23, 1539.
12. Li, Y. Y.; He, J. S.; Qiang, W.; Hu, X. Polymer 2002, 43, 2489.
13. Ishihara, N. Makromol Symp 1995, 89, 553.
14. Reynoids, N. M.; Stidham, H. D.; Hsu, S. L. Macromolecules 1991, 24, 3662.
15. Chen, T. V.; Shyu, G. D.; Isayev, A. I. Polym Eng Sci 1995, 35, 733.
16. Jeziorny, A. Polymer 1987, 19, 1142.
17. Chen, Q. Y.; Yu, Y. N.; Na, T. H.; Zhang, H. F.; Mo, Z. S. Chin J Appl Chem 2002, 19, 827.
18. Paszto, J.; Landes, B. G.; Karjala, P. J. Thermochim Acta 1991, 177, 187.
19. Avrami M. J Chem Phys 1939, 7, 1103.
20. Avrami M. J Chem Phys 1940, 8, 212.
21. Mandelkern, L. Crystallization of Polymers; McGraw Hill: New York, 1964.
22. Tobin, M. C. J Polym Sci Polym Phys Ed 1974, 12, 399.
23. Tobin, M. C. J Polym Sci Polym Phys Ed 1976, 14, 2253.
24. Tobin, M. C. J Polym Sci Polym Phys Ed 1977, 15, 2269.
25. Ziabicki, A. Appl Polym Symp 1967, 6, 1.
26. Ziabicki, A. Polymer 1967, 12, 405.
27. Ziabicki, A. Fundamentals of Fiber Spinning; Wiley: New York, 1976; p 112.
28. Evans, U. R. Trans Faraday Soc 1945, 41, 365.
29. Ozawa, T. Polymer 1971, 12, 150.
30. Liu, T. X.; Mo, Z. S.; Zhang, H. F. J Polym Eng 1998, 18, 283.
31. Liu, S. Y.; Yu, Y. Y.; Cui, Y.; Zhang, H. F.; Mo, Z. S. J Appl Polym Sci 1998, 70, 2371.
32. Zhang, Q. X.; Zhang, Z. H.; Zhang, H. F.; Mo, Z. S. J Polym Sci Part B: Polym Phys 2002, 40, 1784.
33. Kissinger, H. Z. J Res Natl Bur Stand 1956, 57, 217.
34. Vyazovkin, S. J. Comput Chem 1997, 18, 393.
35. Vyazovkin, S. Macromol Rapid Commun 2002, 23, 771.
36. Friedman, H. J Polym Sci Part C: Polym Symp 1965, 6, 183.
37. Cebe, P.; Hong, S. D. Polymer 1986, 27, 1183.
38. Lu, H. B.; Nutt, S. J Appl Polym Sci 2003, 89, 3464.
39. Bu, W. S.; Li, Y. Y.; He, J. S.; Zeng, J. J. Macromolecules 1999, 32, 7224.
40. Ho, R. M.; Lin, C. P.; Tsai, H. Y.; Woo, E. M. Macromolecules 2000, 33, 6517.